

of 10-MHz repetition rate. Low ringing levels and high balances between the positive and negative parts of the monocycle pulses have also been achieved without any circuit tuning. The developed circuits are simple and completely uniplanar and, hence, are attractive for compact low-cost time-domain microwave systems such as subsurface sensing radar.

#### ACKNOWLEDGMENT

The authors wish to thank the anonymous reviewers for their useful comments and suggestions.

#### REFERENCES

- [1] C. William, "High-power microwave generation using optically activated semiconductor switches," *IEEE Trans. Electron Devices*, vol. 37, pp. 2439–2448, Dec. 1990.
- [2] C. H. Lee, "Picosecond optics and microwave technology," *IEEE Trans. Microwave Theory Tech.*, vol. 38, pp. 596–607, May 1990.
- [3] V. G. Shpak *et al.*, "Active former of monocycle high-voltage subnanosecond pulses," in *12th IEEE Pulsed Power Conf. Dig.*, June 1999, pp. 1456–1459.
- [4] J. Millman and H. Taub, *Pulse, Digital, and Switching Waveforms*. New York: McGraw-Hill, 1965, ch. 13, 20.
- [5] J. L. Moll *et al.*, "Physical modeling of the step recovery diode for pulse and harmonic generation circuits," *Proc. IEEE*, vol. 57, pp. 1250–1259, July 1969.
- [6] K. Madani *et al.*, "A 20-GHz microwave sampler," *IEEE Trans. Microwave Theory Tech.*, vol. 40, pp. 1960–1963, Oct. 1992.
- [7] M. J. W. Rodwell *et al.*, "GaAs nonlinear transmission lines for picosecond pulse generation and millimeter-wave sampling," *IEEE Trans. Microwave Theory Tech.*, vol. 39, pp. 1194–1204, July 1991.
- [8] D. Salameh and D. Linton, "Microstrip GaAs nonlinear transmission-line (NLTL) harmonic and pulse generators," *IEEE Trans. Microwave Theory Tech.*, vol. 47, pp. 1118–1121, July 1999.

## An Inverse Technique to Evaluate Permittivity of Material in a Cavity

Kailash P. Thakur and Wayne S Holmes

**Abstract**—A numerical technique to estimate the dielectric constant and loss factor of a homogeneous dielectric material placed in an arbitrary shaped cavity has been developed. The values of *S*-parameters are measured experimentally by placing the sample in the cavity. Starting with a trial set of permittivity values, the computation is carried out using the finite-element method (FEM) to match the *S*-parameters around the fundamental resonance frequency. The FEM routine is run several times while optimizing the values of dielectric constant and conductivity of the sample. During the process of optimization, eight different measures of error between computed and experimental values of complex *S*-parameters are examined. It is found that there is no single measure of error, which can be minimized to estimate two parameters (dielectric constant and the loss factor), but the combination of errors has to be minimized to get the exact solution. The computer program can generate the solution with an accuracy of less than 0.01% in a few hours on a pentium-based personal computer.

**Index Terms**—Cavity resonance, dielectric constant, FEM, inverse problem, Monte Carlo simulation.

### I. INTRODUCTION

The measurement of the dielectric constant and loss factor of a material plays an important role in microwave technology. There are several techniques developed for an accurate measurement of permittivity of the material [1]–[7]. The measurement technique at microwave frequencies can be classified in three groups: 1) by using some probe or microwave sensor; 2) by using a waveguide cell filled with the sample of dielectric, where there is restriction upon the sample size and its alignment in the waveguide cell; and 3) by using the cavity resonance.

In the third group of techniques, the shift in the resonance peak and *Q* values of the cavity with and without the sample generate the values of dielectric constant and loss factor of the sample using the perturbation method. However, there are limitations for the use of the perturbation method. The sample size should be very small compared to the dimension of the cavity so that the electric field inside the cavity does not change much due to the presence of the sample. In a large number of applications it is not always possible to have a sample of acceptable dimensions. For example, if we intend to measure the dielectric constant of an apple, it will not be a good idea to use the perturbation technique.

This paper presents the development of a numerical simulation technique to obtain the complex permittivity (dielectric constant and loss factor) of a dielectric material of an arbitrary shape placed in an arbitrary-shaped cavity by using the finite-element method (FEM). The experimental values of *S*-parameters around the fundamental resonance frequency are matched with the simulated data.

### II. PROCEDURE

In principle, the geometry of the cavity and dimensions of the sample within the cavity has no restriction as long as the entire volume can be divided into discrete elements acceptable by the FEM routine. However, a simple rectangular geometry has been considered here for the

Manuscript received July 11, 2000. This work was supported by the New Zealand Foundation for Research Science and Technology under Contract C08806, Objective 4.

The authors are with the Imaging and Sensing Team, Industrial Research Ltd., Auckland, New Zealand (e-mail: k.thakur@irl.cri.nz).

Publisher Item Identifier S 0018-9480(01)03984-9.

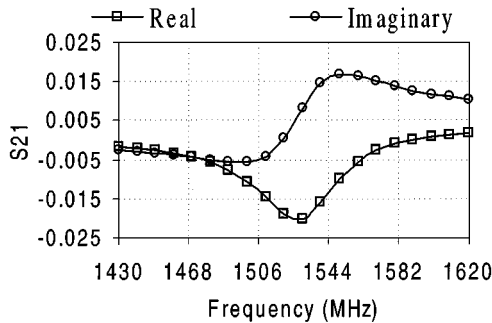


Fig. 1. Real and imaginary components of  $S_{21}$  for the cavity loaded with the dielectric sample.

sake of simplicity. A rectangular cavity of  $15 \text{ cm} \times 12 \text{ cm} \times 9 \text{ cm}$  has been used. The sample is also a rectangular slab ( $2 \text{ cm} \times 3 \text{ cm} \times 3 \text{ cm}$ ), placed at the center of the cavity. In this paper, the measurement process has been simulated by using the direct FEM solution for the sample of known complex permittivity (dielectric constant  $\epsilon_r = 3.709709$  and conductivity  $\sigma = 0.144941 \text{ S/m}$ ) in the frequency range from 1430 to 1620 MHz at the frequency step of 10 MHz. We have used a three-dimensional (3-D) vector FEM method [8], [9] using the complex numbers and the complex biconjugate gradient method [10] for the solution of the 3-D wave equation

$$\nabla \times \left[ \frac{1}{\mu_r} \nabla \times E(r) \right] - k_o^2 \epsilon_r E(r) = -j k_o Z_o J(r) \quad (1)$$

where  $\epsilon_r$  is the complex permittivity of material inside the cavity and the other terms have their usual significance [8]. The electric field  $E(r)$  within an elementary discretized tetrahedral element can be written as

$$E(r) = \sum_{k=1}^6 E_k w_k(r) \quad (2)$$

where  $w_k(r)$  are the weighing functions taken equal to the basis functions in Galerkin's formulism, and  $E_k$  are complex coefficients. The representation of the whole problem in the matrix form can be obtained by multiplying (1) by  $w_k(r)$  and integrating over the elementary volume and using (2) as follows:

$$[A] [E] = [B] \quad (3)$$

where

$$A_{ij} = \int \left[ \frac{1}{\mu_r} \left( \nabla \times w_i(r) \right) \cdot \left( \nabla \times w_j(r) \right) - j k_o Z_o \epsilon_r w_i(r) \cdot w_j(r) \right] dv \quad (4)$$

and

$$B_i = \int J_i(r) \cdot w_i(r) dS. \quad (5)$$

When a dielectric sample is placed in the cavity, the matrix  $[A]$  in (3) splits up into two matrices corresponding to two different sets of complex permittivities. The electric field around the input port is known and, thus, are some components of complex vector  $[E]$  in (3). Therefore, all unknown field elements of (3) can be obtained. The simulated measurement results for the loaded cavity is shown in Fig. 1.

### III. ERROR MINIMIZATION

The computational steps involved in obtaining the unknown complex permittivity of dielectric sample in the cavity are shown in Fig. 2. The forward computations are carried out to obtain  $S_{21}$  for the cavity loaded with the dielectric sample of same size, but having known values of complex permittivity. The objective here is to match the computed and experimental values of the  $S_{21}$  parameter at all measured frequency around the resonance peak. In order to match the  $S_{21}$  parameters and, hence, obtain the complex permittivity of the sample, we start with an initial trial value of complex permittivity, get the final FEM results, and compute the error with respect to the experimental data. Repeat the process for some different values of complex permittivity and compute the error again. The process of this optimization is done using a restricted Monte Carlo simulation. From the knowledge of the nature of dependence of error upon permittivity of the material, the restriction upon the next iteration is imposed so that the search is carried out in the right direction.

However, the problem here is how accurately one can obtain the location of the resonance peak and its height from the available data at a discrete frequency. Using different extrapolation techniques generates different results, which restrict the accuracy of the prediction process. Moreover, there is limitation of FEM computations upon the termination of iterative computations of roots using the complex biconjugate gradient method, which can be terminated if the error is less than some tolerance error and yields different errors at different frequencies. This makes some results more accurate than the other. In this paper, eight different measures of error ( $\varepsilon_1$ — $\varepsilon_8$ ) between the experimental and computed values of  $S$ -parameters are estimated as follows:

$$\begin{aligned} \varepsilon_1 &= \frac{(F_e - F_c)}{F_e} \\ \varepsilon_2 &= \frac{(S_{21e} - S_{21c})}{S_{21e}} \\ \varepsilon_3 &= \frac{(FL_e - FL_c)}{FL_e} \\ \varepsilon_4 &= \frac{(Q_e - Q_c)}{Q_e} \\ \varepsilon_5 &= \frac{(FR_e - FR_c)}{FR_e} \\ \varepsilon_6 &= \frac{(S_{21Re} - S_{21Rc})}{S_{21Re}} \\ \varepsilon_7 &= \frac{(FP_e - FP_c)}{FP_e} \\ \varepsilon_8 &= \frac{(A_e - A_c)}{A_e} \end{aligned} \quad (6)$$

where

$F_e$  and  $F_c$

experimental and computed frequencies of the maximum absolute value of real component of  $S_{21}$ , respectively;

$S_{21e}$  and  $S_{21c}$

experimental and computed values of the maximum absolute value of the real component of  $S_{21}$ , respectively;

$FL_e$  and  $FL_c$

experimental and computed values of resonance frequency for  $S_{21}$ , obtained from Lorenz curve fitting, respectively;

$Q_e$  and  $Q_c$

experimental and computed values of  $Q$  for  $S_{21}$  obtained from Lorentz curve fitting, respectively;

$FR_e$  and  $FR_c$

experimental and computed values of resonance frequency of  $S_{21}$  obtained from simple quadratic regression of five data points around the peak, respectively;

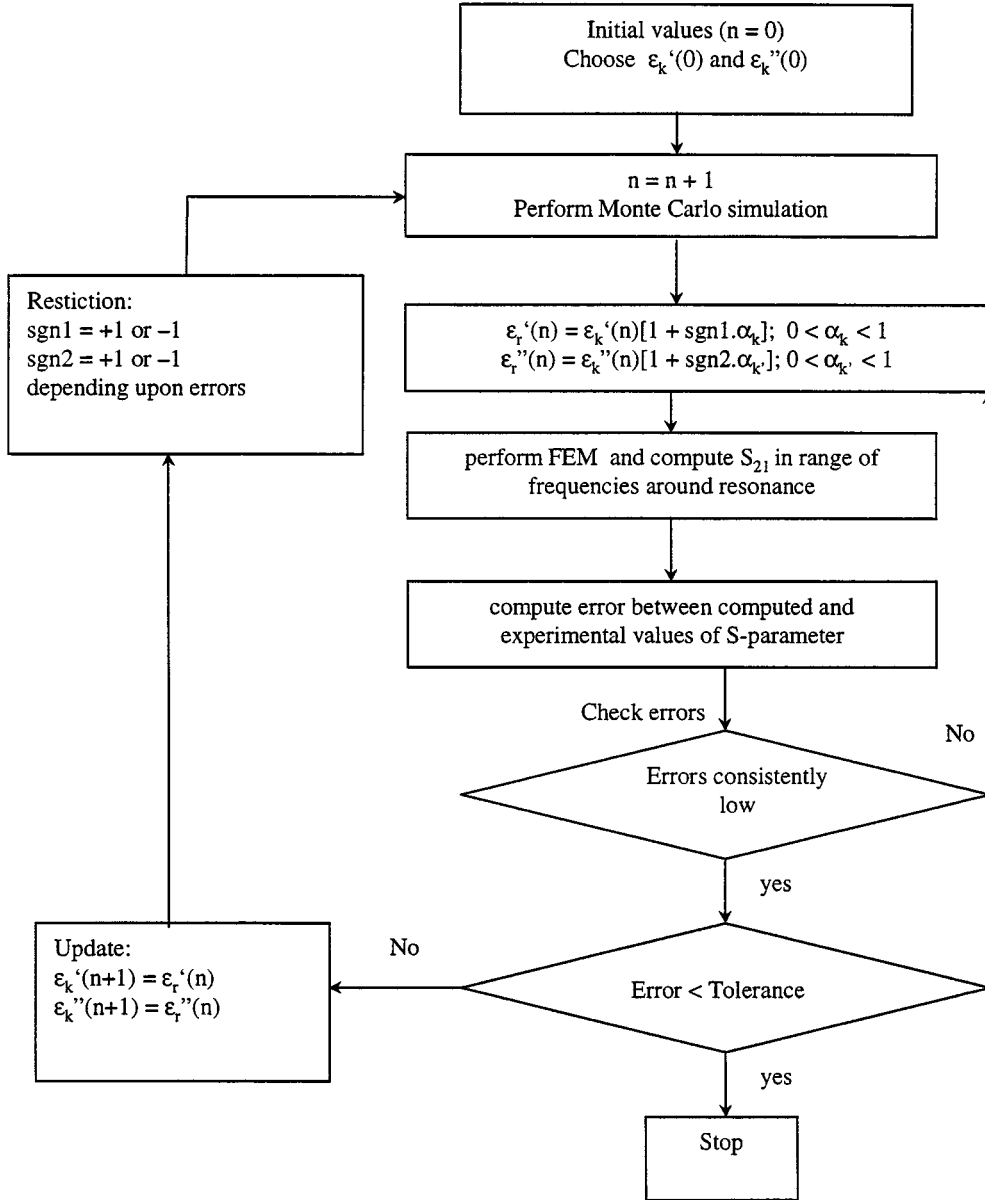


Fig. 2. Procedure for coupling the FEM and restricted Monte Carlo technique.

$S_{21Re}$  and  
 $S_{21Rc}$

experimental and computed values of the height of the resonance peak obtained from simple quadratic regression of five data points around the peak, respectively;

$FP_e$  and  $FP_c$

experimental and computed values of frequency at which there is an abrupt change of phase ( $= \pi$ ) around the resonance peak of  $S_{21}$ , respectively;

$A_e$  and  $A_c$

experimental and computed values of the area intercepted by  $S_{21}$  on the frequency axis, respectively.

These errors fall into two groups: 1)  $Err1 = \epsilon_1 + \epsilon_3 + \epsilon_5 + \epsilon_7$  and 2)  $Err2 = \epsilon_2 + \epsilon_4 + \epsilon_6 + \epsilon_8$ . In the present simulation technique, all eight errors are minimized simultaneously. If errors of the same group differ considerably from each other (one positive and the other negative), the current results are discarded and the next iteration proceeds with the earlier data. The convergence is very fast and depends upon the initial values of the complex permittivity.

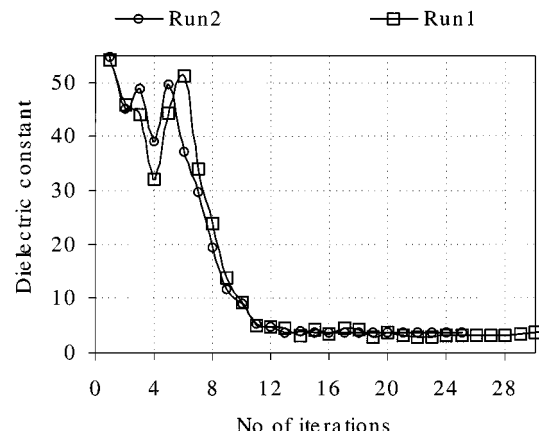


Fig. 3. Convergence of the simulation processes for two different runs for dielectric constant.

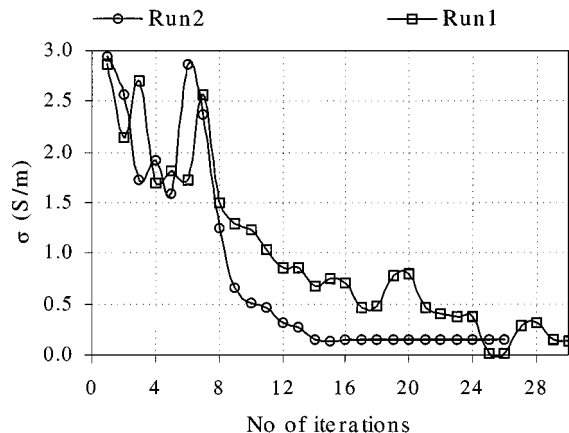


Fig. 4. Convergence of the simulation processes for two different runs for conductivity  $\sigma$ .

Several runs were made and the results of the convergence of two runs are shown in Figs. 3 and 4. After the convergence is reached, the simulated curve for  $S_{21}$  matched exactly with the experimental one of Fig. 1, and the permittivity of the sample is reproduced with an accuracy of 0.01%.

#### IV. CONCLUSION

Based upon the FEM and a cavity resonance technique, an iterative method for exact estimation of complex permittivity of an arbitrary shaped dielectric has been presented. The measurements are done in a frequency band around any resonance peak, preferably the fundamental one. This paper also defined a number of error parameters used in the process of optimization. The technique can be implemented very easily on a desktop computer for a quick estimation of permittivity of samples on the production line.

#### ACKNOWLEDGMENT

The authors wish to thank Prof. A. G. Williamson, University of Auckland, New Zealand, and Dr. K. L. Chan, Industrial Research Ltd., Auckland, New Zealand, for critically reading this paper's manuscript.

#### REFERENCES

- [1] M. N. Afsar, J. R. Birch, and R. N. Clarke, "The measurement of the properties of materials," *Proc IEEE*, vol. 74, pp. 183–199, MONTH 1986.
- [2] W. E. Courtney, "Analysis and evaluation of a method of measuring the complex permittivity and permeability of microwave insulators," *IEEE Trans. Microwave Theory Tech.*, vol. MTT-18, pp. 476–485, MONTH 1970.
- [3] R. A. Waldron, "Perturbation theory of resonant cavities," *Proc. Inst. Elect. Eng.*, vol. 107C, pp. 272–274, MONTH 1960.
- [4] D. Aregba, J. Gay, and G. Maze-Merceur, "Modeling multiport using a three-dimensional coupled analytical/finite element method application to microwave characterization of material," *IEEE Trans. Microwave Theory Tech.*, vol. 42, pp. 590–4, Apr. 1994.
- [5] R. Cocciali, G. Pelosi, and S. Selleri, "Characterization of dielectric materials with the finite-element method," *IEEE Trans. Microwave Theory Tech.*, vol. 47, pp. 1106–1111, July 1999.
- [6] B. Meng, J. Booske, and R. Cooper, "Extended cavity perturbation technique to determine the complex permittivity of dielectric materials," *IEEE Trans. Microwave Theory Tech.*, vol. 43, pp. 2633–2636, Dec. 1994.

- [7] J. K. Vaid, A. Prakash, and A. Mansingh, "Measurement of dielectric parameters at microwave frequencies by cavity perturbation technique," *IEEE Trans. Microwave Theory Tech.*, vol. MTT-27, pp. 791–795, Sept. 1979.
- [8] J. M. Jim, *The Finite Element Method in Electromagnetics*. New York: Wiley, 1993.
- [9] R. Miniowitz and J. P. Webb, "Analysis of 3-D microwave resonators using covariant-projections elements," *IEEE Trans. Microwave Theory Tech.*, vol. 39, pp. 1895–1899, Nov. 1991.
- [10] D. A. H. Jacobs, "A generalization of the conjugate gradient method to solve complex systems," *IMA J. Numer. Anal.*, vol. 6, pp. 447–452, 1986.

## A Full-Wave Modal Analysis of Inhomogeneous Waveguide Discontinuities with Both Planar and Circular Cylindrical Boundaries

Robert H. MacPhie and Ke-Li Wu

**Abstract**—A full-wave analysis of an inhomogeneous waveguide region with both planar and circular cylindrical boundaries is presented in this paper. Circular cylindrical modal functions are used to represent the fields. Field matching on the planar walls and apertures is rigorously achieved by the finite plane-wave series expansion of each modal field, whereas the addition theorem for cylindrical waves is used for rigorous field matching on the circular cylindrical boundaries. Numerical results are given for rectangular waveguides with 90° bends and rounded outer corners.

**Index Terms**—Full-wave modal analysis, inhomogeneous waveguide functions.

#### I. INTRODUCTION

In a recent paper [1], MacPhie and Wu provided a full-wave modal analysis of waveguide discontinuities with piecewise planar boundaries. Practical examples of such discontinuities are T-, Y-junctions and *E*- and *H*-plane mitered 90° bends. In this paper, this technique is extended to discontinuities with both planar and circular cylindrical boundaries. Such an inhomogeneous waveguide discontinuity is shown in Fig. 1, where there are two feeding waveguides, four planar sidewalls, and two circular cylindrical sidewalls. As in [1], the height of the region is  $w$  with bottom and top walls at  $z = 0$  and  $z = w$ , respectively.

Bessel-Fourier modal functions are used to represent the TM- ( $e$ ) and TE-type ( $h$ ) fields in the inhomogeneous region [1], [2]. For field matching in the planar waveguide apertures  $A_n$  and on the planar sidewalls  $W_m$ , the finite plane-wave series expansion [1] is employed. However, on the circular cylindrical walls  $C_l$ , a rigorous solution is obtained by means of the translation addition theorem [3] for circular cylindrical wave functions. The proposed formula is verified by the comparison of the numerical results obtained by the finite-element method (FEM) and those of the proposed modal analysis for WR75 waveguide 90° bends (both *H*- and *E*-planes) having rounded outer corners.

Manuscript received April 26, 2000.

R. H. MacPhie is with the Department of Electrical and Computer Engineering, University of Waterloo, Waterloo, ON N2L 3G1, Canada.

K.-L. Wu is with the Department of Electronic Engineering, The Chinese University of Hong Kong, Shatin, Hong Kong.

Publisher Item Identifier S 0018-9480(01)03981-3.